

The Smoking Guns of Neutron Stars Mergers

Shlomo Dado and Arnon Dar
Physics Department, Technion, Haifa, Israel

The short hard gamma ray burst (SHB) 170817A that followed GW170817A, the first neutron stars merger (NSM) detected in gravitational waves (GWs), has shown beyond doubt that NSMs produce beamed SHBs. Its low luminosity and other properties that differ from those of ordinary SHBs were predicted by the cannonball model of gamma ray bursts. Low luminosity (LL) SHBs are mainly ordinary SHBs viewed far off-axis. They are produced mainly by nearby NSMs. Because of beaming, most of the NSMs, including those within the current horizon of Ligo-Virgo, produce SHBs most of which are invisible from Earth. But, their pulsar wind nebula powered by the spin down of the remnant neutron star produces an early-time isotropic afterglow with a universal temporal shape. This smoking gun of NSMs is detectable independent of whether the SHB was visible, or was invisible from Earth because of being beamed away.

PACS numbers:

I. INTRODUCTION

Gamma-ray bursts (GRBs) are brief flashes of gamma rays lasting between few milliseconds and several hours [1] from extremely energetic cosmic explosions [2]. They were first detected in 1967 by the USA Vela satellites. Their discovery was published in 1973 after 15 such events were detected [3]. Since 1967, the origin and production mechanism of GRBs have been among the major puzzles in astrophysics.

GRBs fall roughly into two classes [4], long duration ones (long GRBs) that last more than ~ 2 seconds, and short hard bursts (SHBs) that typically last less than 2 seconds. For the first 3 decades after their discovery, the origin of both types of GRBs were completely unknown. This has changed dramatically after the launch of the BeppoSAX satellite in 1996. Its sky localization of GRBs and its discovery of their X-ray afterglow [5] led to the discovery of their afterglow at longer wavelengths [6,7], which led to the discovery of GRB host galaxies [8] and their typical redshifts [9], and the association of **long GRBs** with supernova (SN) explosions of type Ic [10]. Following measurement during the past 20 years, mainly with the X-ray satellites HETE, Swift, Konus-Wind, Chandra, Integral, XMM-Newton, and Fermi, with the Hubble space telescope, and with ground based telescopes, provided the detailed properties of the prompt and afterglow emissions of GRBs over the entire electromagnetic spectrum. They also provided information on their host galaxies, their location and environment within their hosts, and their production rate as function of redshift.

Progress in identifying the origin and production mechanism of SHBs was much slower. Until recently, SHBs were believed [11] to be produced in merger of neutron stars [12,13] and in neutron star-black hole mergers [14] in compact binaries. This belief was based on indirect evidence [12]. Recently, however, SHB170817A [15,16] that followed 1.7s after the chirp of the gravitational wave (GW) emission from the relatively nearby neutron stars merger (NSM) event GW170817 detected with the Ligo-

Virgo GW detectors [17-19], has shown beyond doubt that NSMs produce SHBs. SHB170817A however, appeared to be different from all SHBs observed before it [11]. But, using the Cannonball (CB) model of GRBs [20-22], we have shown, as detailed below that SHB170817A was an ordinary SHB whose properties appeared to be different from ordinary SHBs because it was viewed from far off-axis.

The properties of the far off-axis SHBs and their early afterglow, associated with NSMs detected by the current Ligo-Virgo detectors, were predicted [23] before the GW170817-SHB170817A event. In the CB model, SHBs are highly beamed. NSM events within the detection horizon of Ligo-Virgo produce mostly far off-axis SHBs. Such far off-axis SHBs, if detected, have a much lower luminosity than that of ordinary near axis SHBs.

The emission of the nebula surrounding the NSMs that is powered by the spin down of the newly born neutron star remnant, is isotropic. It dominates the early time afterglow of all SHBs, independent on whether the SHB is viewed from near axis or from far-off axis [24].

The late-time beamed afterglow of SHBs is usually too faint to be visible, unless the SHB is very nearby, such as SHB 170817A. The behavior of such a far off-axis beamed afterglow is also well predicted by the CB model of SHBs [25].

II. UNIVERSAL PROPERTIES OF SHBS

On August 17, 2017, GW170817, the first neutron star merger event was detected in gravitational waves by Ligo-Virgo [17]. It was followed by a short gamma ray burst, SHB170817A, detected by the Fermi [15,26] and Integral [16] satellites, 1.74 ± 0.05 s after the chirp ending the arrival of gravitational waves. It was the first indisputable NSM-SHB association, indicating that SHBs probably are produced by NSMs. This is despite the fact that SHB170817A [26] and its *late-time* X-ray [27] and radio [28] afterglows look very different from SHBs and their X-ray and radio afterglows, which were observed

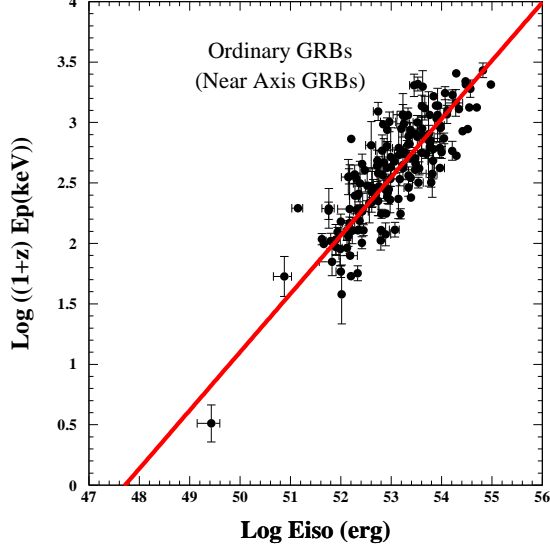


FIG. 1: The peak energy in the GRB rest frame as a function of the isotropic equivalent total gamma ray energy of ordinary GRBs viewed near axis. The line is the correlation predicted by the CB model as given by Eq.(1).

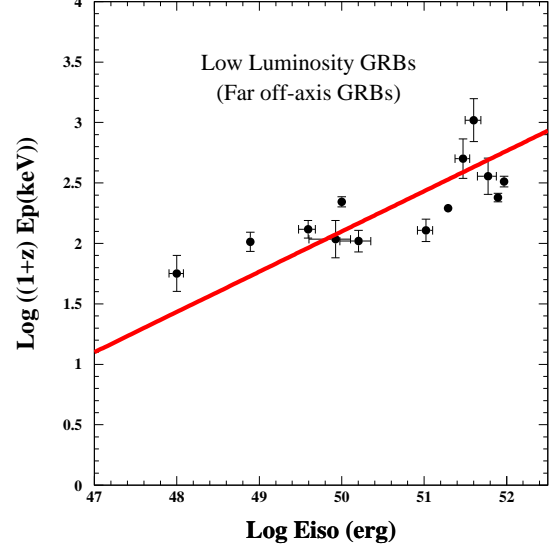


FIG. 2: The $[E_p, E_{iso}]$ correlation in low luminosity (far off-axis) LGRBs. The line is the CB model prediction as given by Eq.(2).

before [12].

A. Prompt Emission Correlations

In the CB model, GRBs and SHBs are produced by inverse Compton scattering (ICS) of glory photons by a narrow jet of CBs with a large bulk motion Lorentz factor $\gamma \gg 1$ launched by a central engine. The glory—an ambient light surrounding the launch site—has a cutoff power law (CPL) spectrum, $\epsilon (dn/d\epsilon) \propto \epsilon^{1-\alpha} \exp(-\epsilon/\epsilon_p)$. For a burst at redshift z and a viewing angle $\theta^2 \ll 1$, and $\alpha \approx 1$ the peak energy of their time-integrated energy spectrum satisfies $(1+z) E_p \propto \gamma \delta$, and their isotropic-equivalent total gamma-ray energy satisfies $E_{iso} \propto \gamma \delta^3$ [29], where the Doppler factor $\delta = 1/\gamma(1 - \beta \cos\theta)$ satisfies to a good approximation, $\delta \approx 2\gamma/(1 + \gamma^2\theta^2)$. Hence, assuming that GRBs and SHBs are roughly standard candles in their rest frame, GRBs and SHBs that are mostly viewed from an angle $\theta \approx 1/\gamma$, satisfy

$$(1+z) E_p \propto [E_{iso}]^{1/2}, \quad (1)$$

while far off-axis ($\theta^2 \gg 1/\gamma^2$) SHBs satisfy

$$(1+z) E_p \propto [E_{iso}]^{1/3}. \quad (2)$$

The above correlations are well satisfied by GRBs [25] as shown in Figures 1,2.

As shown in Figure 3, SHBs appear to obey Eq.(1), as expected from ordinary (OR) near axis ($\gamma\theta \approx 1$) SHBs. If, however, SHB170817A were an ordinary standard candle

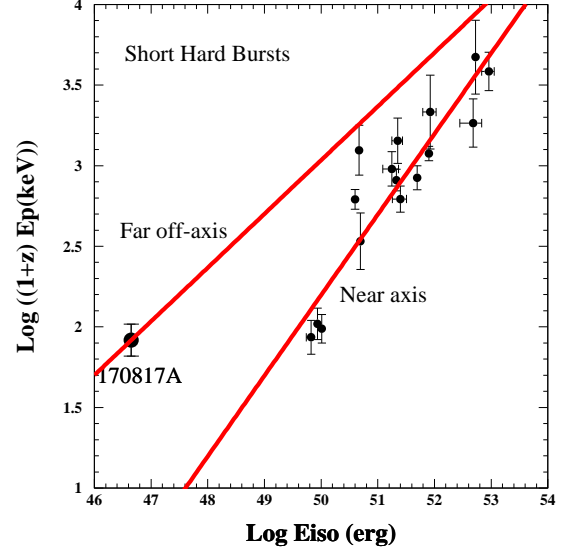


FIG. 3: The $[E_p, E_{iso}]$ correlations in SHBs. The lines are the CB model predictions given by Eqs (1) and (2).

SHB viewed from a far off-axis angle θ , then its E_{iso} and E_p should have satisfied,

$$E_{iso} \approx \langle E_{iso}(OR) \rangle / [\gamma^2 (1 - \cos\theta)]^3, \quad (3)$$

and

$$(1+z) E_p \approx \langle (1+z) E_p(OR) \rangle / [\gamma^2 (1 - \cos\theta)]. \quad (4)$$

Indeed, the very small $E_{iso} \approx 5.6 \times 10^{46}$ erg of SHB170817A [26] relative to the mean $\langle E_{iso} \rangle \approx 1 \times 10^{51}$

erg of OR SHBs, as given by Eq.(3), yields $\gamma\theta \approx 7.2$. Assuming the same redshift distribution of GRBs and SHBs with a mean value $z \approx 2$, and $\langle E_p \rangle = 650$ keV [30] yields $\langle (1+z) E_p \rangle \approx 1950$ keV. Consequently, Eq.(4) with $\gamma\theta \approx 7.2$ yields $(1+z) E_p \approx 75$ keV for SHB170817A, in agreement with the value $(1+z) E_p = 82 \pm 23$ keV (T_{90}) reported in [15] and $E_p \approx 65 + 35 / -14$ keV, estimated in [31] from the same data. This seems to confirm that SHB170817A was an ordinary SHB viewed from a far off-axis. A more direct confirmation is provided [32] by the reported apparent superluminal velocity of its late-time radio afterglow [33].

B. Pulse Shape

SHBs, like long GRBs, are a superposition of pulses produced by a jet of CBs by ICS of glory photons with a CPL spectrum, Their time sequence is unpredictable, but their shape is predictable. It is given approximately by [21].

$$E \frac{d^2 N_\gamma}{dE dt} \propto \frac{t^2}{(t^2 + \Delta^2)^2} E^{1-\alpha} \exp(-E/E_p(t)) \quad (5)$$

where Δ is approximately the pulse peak time in the observer frame, which occurs when the CB becomes transparent to its radiation, and $E_p \approx E_p(t = \Delta)$. In Eq.(5), the early-time temporal rise like t^2 is produced by the increasing cross section, $\pi R_{CB}^2 \propto t^2$, of the fast expanding CB of a radius R_{CB} when the CB is still opaque to radiation. When the CB becomes transparent to radiation due to its fast expansion, its effective cross section for ICS becomes a constant equal to the Thomson cross section times the number of electrons in the CB. That, and the density of the glory photons, which far from the launch point decreases like $n_g(r) \propto 1/r^2 \propto t^{-2}$, produce the temporal decline like t^{-2} . If CBs are launched along the axis of an accretion disk or a torus with a radius R_g , then glory photons that intercept the CB at a distance r from the center have an incident angle θ_{inc} , which satisfies $\cos \theta_{inc} = -r / \sqrt{r^2 + R_g^2}$. This yields a t -dependent peak energy of the photons undergoing ICS, $E_p(t) = E_p(0)(1 - t/\sqrt{t^2 + \tau^2})$ with $\tau = R_g(1+z)/\gamma \delta c$, and $E_p \approx E_p(t \approx \Delta)$.

For GRBs/SHBs with $\tau \gg \Delta$, Eq.(5) yields half maximum values at $t \approx 0.41 \Delta$ and $t = 2.41 \Delta$, which yield a full width at half maximum $FWHM \approx 2 \Delta$, a rise time from half maximum to peak value $RT = 0.59 \Delta$, and a decay time from peak count to half peak, $DT = 1.41 \Delta$. Consequently $RT/DT \approx 0.42$ and $RT \approx 0.30 FWHM$.

In Figure 4 we compare the measured shape [26] of the first prompt emission pulse of SHB170817A and the CB model pulse shape as given by Eq.(5) with the best fit parameters $\Delta = 0.62$ s and $\tau = 0.57$ s ($\chi^2/dof = 0.95$). The best fit light curve has a maximum at $t = 0.43$ s, a half maximum value at $t = 0.215$ s and $t = 0.855$ s, an asymmetry $RT/DT = 0.50$ and $RT/FWHM = 0.34$.

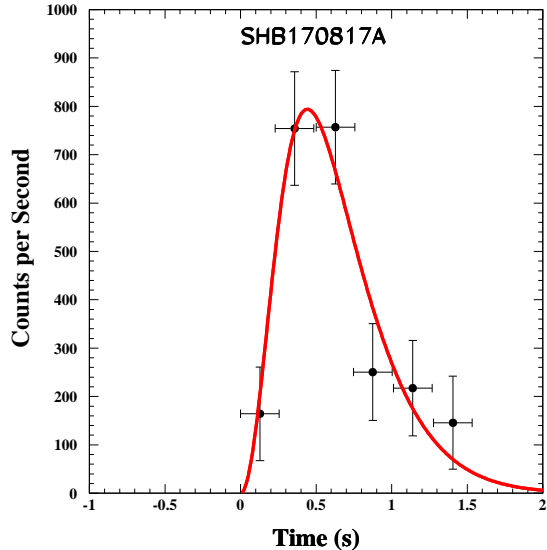


FIG. 4: The pulse shape of SHB170817A measured with the Fermi-GBM [26] and the best fit pulse shape given by Eq.(6) with $\Delta = 0.62$ s and $\tau = 0.57$ s.

C. Early-Time Universal Afterglow

As long as the spin-down of a pulsar with a period $P(t)$ satisfies $\dot{P}P = const$,

$$P(t) = P_i(1 + t/t_b)^{1/2}, \quad (6)$$

where $P_i = P(0)$ is the initial period of the pulsar, t is the time after its birth, and $t_b = P_i/2 \dot{P}_i$. If a constant fraction η of the rotational energy loss of such pulsar is reradiated by the pulsar wind nebula (PWN), then, in a steady state, its luminosity satisfies $L = \eta I \dot{\omega}$, where $\omega = 2\pi/P$ and I is the moment of inertia of the neutron star. Hence, in a steady state, the luminosity emitted by a PWN satisfies

$$L(t) = L(0)/(1 + t/t_b)^2. \quad (7)$$

Eq.(7) can be written as

$$L(t)/L(0) = 1/(1 + t_s)^2, \quad (8)$$

where $t_s = t/t_b$. Thus, the dimensionless luminosity $L(t)/L(0)$ has a simple universal form as function of the scaled time t_s . For each afterglow of an SN-less GRB (long or short) powered by a pulsar, $L(0)$ and t_b can be obtained from a best fit of Eq.(7) to the light curve of their measured afterglow.

Eqs.(7),(8) are expected to be valid only after the last mass accretion episode on the newly born pulsar, and after the PWN emission powered by the pulsar's power supply has reached a steady state. Since the exact times of both are not known, and in order to avoid a contribution from the prompt emission, we have fitted the observed afterglows of SHBs with Eqs.(7),(8) only well after

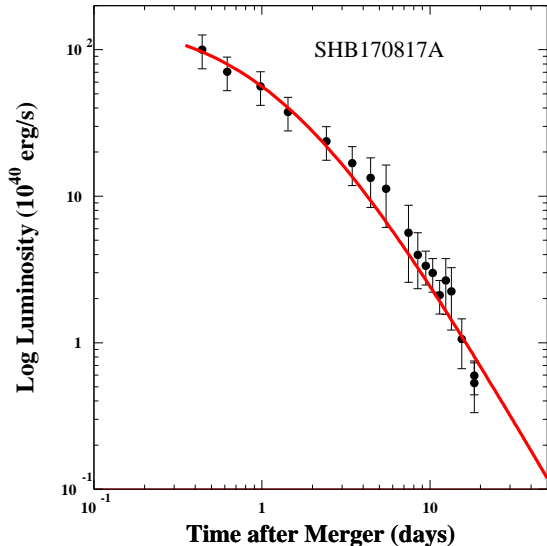


FIG. 5: The best fit CB model lightcurve to the observed bolometric lightcurve of SHB170817A [34], assuming a PWN emission powered by the spin down of a neutron star remnant.

the fast decline of the prompt emission (last pulse/flare or extended emission). This also made unimportant the lack of knowledge of the exact time of the beginning of power supply by the millisecond pulsar (MSP). The observed early-time bolometric afterglow of SHB170817A [34] and its best fit Eq.(7) are shown in Figure 5.

The initial period of the pulsar enshrouded within a PWN can be estimated from its locally measured energy flux $F(0)$ corrected for absorption along the line of sight to the PWN, its redshift z , and its luminosity distance D_L ,

$$P_i = \frac{1}{D_L} \sqrt{\frac{(1+z)\eta\pi I}{2F(0)t_b}}, \quad (9)$$

where $F = L/4\pi D_L^2$, $I \approx (2/5)MR^2 \approx 1.12 \times 10^{45} \text{ g cm}^2$, for a canonical pulsar with $R=10 \text{ km}$ and $M \approx 1.4 M_\odot$, and $\eta < 1$. The period derivative can be obtained from the relation $\dot{P}_i = P_i/2t_b$.

Eqs.(7),(8) are expected to be valid only after the last accretion episode on the newly born pulsar, and after the PWN emission powered by the pulsar's power supply has reached a steady state. Since the exact times of both are not known, and in order to avoid a contribution from the prompt emission, we have fitted the observed early time afterglows of SHBs with Eq.(8) only well after the fast decline of the prompt emission (last pulse/flare or extended emission). This also made unimportant the lack of knowledge of the beginning time of the power supply by the MSP.

In Figure 6 we plotted the dimensionless X-ray afterglow of 12 SHBs with the sampled afterglows measured with the Swift XRT [35] in the first couple of days after

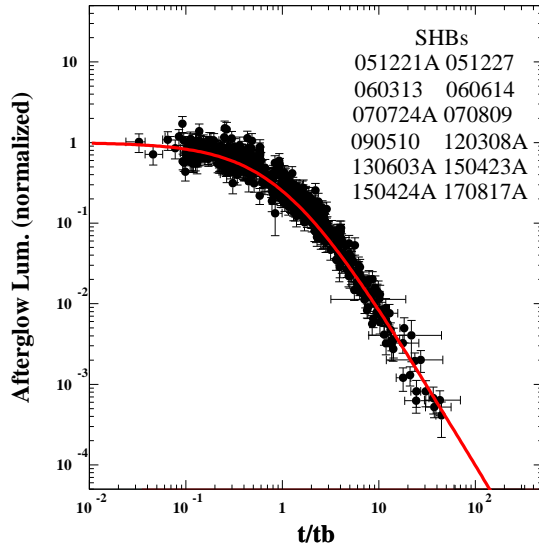


FIG. 6: Comparison between the normalized light curve of the X-ray afterglow of 12 SHBs with a well sampled afterglow, measured with the Swift XRT [35] during the first couple of days after burst and the predicted universal behavior given by Eq.(8). The bolometric light curve of SHB170817A is also included.

TABLE I:

SHB	z	$F_X(0)$ [erg/s cm^2]	t_b [s]	χ^2/dof	P [ms]
051221A	0.5465	2.33E-12	46276	1.04	16.2
051227	0.8	1.44E-11	2280	0.93	19.8
060313		2.91E-11	4482	0.60	
060614	0.125	1.11E-11	48931	1.39	33.2
070724A	0.457	1.18E-12	18041	1.46	43.7
070809	0.2187	3.231E-12	17181	1.05	57.6
090510	0.903	3.68E-10	551	1.76	7.04
120308A		6.84E-11	4742	1.51	
130603B	0.3564	6.25E-12	34382	1.19	17.8
150423A	1.394	1.31E-11	1290	1.36	16.0
150424A	0.30	5.15E-12	34461	1.51	23.5
170817	0.0093		117374	0.60	

burst and the universal behavior given by Eq.(8). The values of $L(0)$ and t_b needed to reduce each measured lightcurve to the dimensionless form were obtained for each SHB from a best fit of Eq.(7) to the observed plateau followed by a fast decline phase of the X-ray afterglow.

The values of P_i and t_b for the 11 SHBs with a well sampled early time X-ray afterglow are listed in Table I.

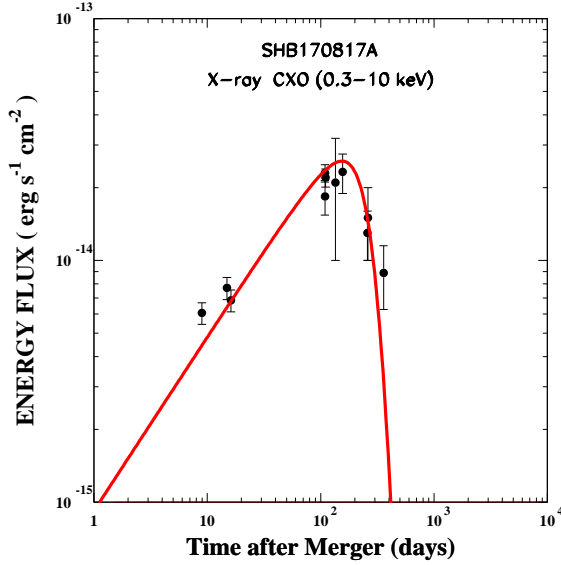


FIG. 7: The lightcurve of the X-ray afterglow of SHB170817A measured with the CXO [27] and the lightcurve predicted by eq.(11) for $\beta_x = 0.56$, and the best fit parameters $t_e = 245.6$ d and $w = 63.4$ d.

D. The Late-time Afterglow of SHB170817A

In the CB model, the observed spectral energy density of the unabsorbed synchrotron afterglow produced by a CB is given by

$$F_\nu \propto n^{(\beta_x+1)/2} [\gamma(t)]^{3\beta_x-1} [\delta(t)]^{\beta_x+3} \nu^{-\beta_x}, \quad (10)$$

where n is the baryon density of the external medium encountered by the CB at a time t and β_x is the spectral index of the emitted X-rays, $E dn_x/dE \propto E^{-\beta_x}$. For a constant density, the deceleration of the CB yields a late-time $\gamma(t) \propto t^{-1/4}$ and as long as $\gamma^2 \gg 1$, $\beta \approx 1$ and $\delta(t) \propto t^{-1/4}/(1 - \cos\theta)$. Consequently, the apparent superluminal velocity of a far off-axis CB in a constant low-density environment, stays constant, as long as $\beta \approx 1$, while its late-time spectral luminosity increases like $t^{(1-\beta_\nu/2)}$. When the CB exits the disk into the halo, it turns into a fast decay $\propto [n(r)]^{(1+\beta_\nu)/2}$. Approximating the disk density perpendicular to the disk by $n(h) = 2n(0)/(1 + \exp(h/d))$ where d is the "skin depth" of the disk, the lightcurve of the afterglow of SHB170817A can be approximated by,

$$F_\nu(t) \propto \frac{(t/t_e)^{1-\beta_\nu/2} \nu^{-\beta_\nu}}{[1 + \exp[(t-t_e)/w]]^{(1+\beta_\nu)/2}} \quad (11)$$

where t_e is roughly the escape time of the CB from the galactic disk into the halo after its launch. Eq.(11) is compared to the observed late-time X-ray [27] and radio [28] afterglows of SHB170817A in Figures 7 and 8, respectively.

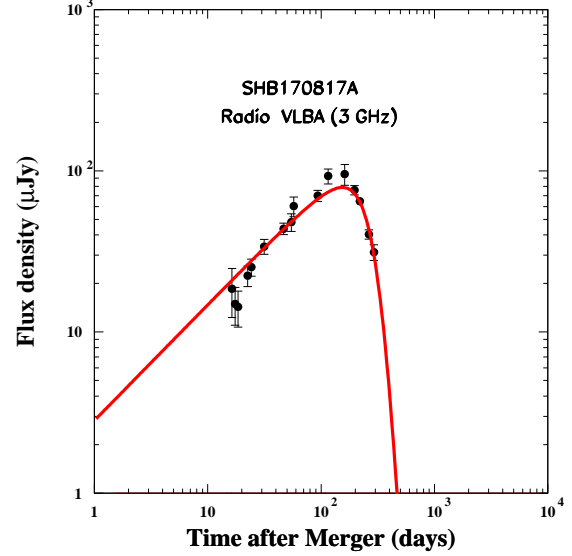


FIG. 8: Left: The measured [28] lightcurve of the 3 GHz radio afterglow of SHB170817A and the lightcurve predicted by the CB mode $\beta_r = 0.56$, $t_e = 245.6$ d and $w = 63.4$ d.

E. Superluminal Radio Afterglow of SHB170817A

The VLA and VLBI localization of the source of the late time radio afterglow of SHB170817A [33] provided the first successful measurement of the apparent superluminal motion of the highly relativistic CBs, which produce the prompt emission and beamed afterglow of GRBs and SHBs (two decades after the discovery of the afterglow of GRBs at lower frequencies [5-7]).

The apparent velocity in the plane of the sky of a highly relativistic compact (unresolved) source moving at a small redshift ($1+z \approx 1$) with a **constant** bulk motion Lorentz factor $\gamma \gg 1$ viewed from an angle θ relative to its direction of motion, is given by

$$V_{app} = \beta \gamma \delta c \sin\theta / (1+z) \approx \frac{c \sin\theta}{(1+z)(1-\cos\theta)}, \quad (12)$$

which depends only on θ . In that case, the angular distance to the afterglow source $D_A \approx V_{app} \Delta t / (1+z) \Delta\theta_s$, and the angular change $\Delta\theta_s$ in the sky location of the source yield

$$\frac{\sin\theta}{(1-\cos\theta)} \approx \frac{\Delta\theta_s D_A (1+z)}{c \Delta t} \quad (13)$$

In the case of SHB170817A in NGC 4993 at redshift $z = 0.009783$ [36], the angular location of the radio source in the plane of the sky has changed during $\Delta t = 155$ days (between day 75 and day 230) by $\Delta\theta_s = 2.68 \pm 0.3$ mas [33]. Thus, assuming the local value of H_0 , 73.52 ± 1.62 km/s Mpc [37], i.e., $D_A \approx 39.43$ Mpc, Eq.(12) yields $\theta \approx 28 \pm 2$ deg ($V_{app} \approx (4.0 \pm 0.4)c$). This value of θ is in agreement with the value 25 ± 4 deg, which was obtained

[38] from GW170817 and its electromagnetic localization [15,26] assuming the local value of H_0 obtained [37] from Type Ia supernovae (SNeIa).

III. CONCLUSIONS

Ordinary SHBs are visible up to very large cosmological distances. They are produced mostly by neutron star mergers whose rotational axis points near the direction of Earth. Low luminosity SHBs are produced by nearby neutron star mergers whose rotational axis points far off the direction of Earth. Only a small fraction of NSMs

within the current detection horizon of Ligo-Virgo produce SHBS visible from Earth. However, all mergers that end with a pulsating neutron star remnant and a visible or an invisible SHB produce **an early-time isotropic afterglow -the smoking gun of NSMs**. These early time afterglows are powered by the spin-down of the remnant neutron star. They have a universal temporal behavior common to ordinary SHBs, far off-axis SHBs, and invisible (very far off-axis SHBs), and are visible up to very large cosmological distances

References

-
- [1] G.J. Fishman, C.A. Meegan, *ARA&A*, 33 (1995) 415.
[2] C.A. Meegan, *et al.*, *Nature*, 355 (1992) 143.
[3] R.W. Klebesadel, I.B. Strong, R.A. Olson, *ApJ*, 182 (1973) L85.
[4] J. P. Norris, *et al.*, *Nature*, 308 (1984) 434.
[5] E. Costa, *et al.*, *Nature*, 387 (1987) 783 [arXiv:astro-ph/9706065].
[6] J. van Paradijs, *et al.*, *Nature*, 386 (1997) 686.
[7] D.A. Frail, *et al.*, *Nature*, 389 (1997) 261.
[8] K.C. Sahu, *et al.*, *Nature*, 387 (1997) 476 [arXiv:astro-ph/9705184].
[9] M.R. Metzger, *et al.*, *Nature*, 387 (1997) 878.
[10] T.J. Galama, *et al.*, *ApJ*, 536 (2000) 185 [arXiv:astro-ph/9907264].
[11] E. Berger, *ARA&A*, 52 (2014) 43 [arXiv:1311.2603].
[12] S.I. Blinnikov, *et al.*, *SvAL*, 10 (1984) 177 [arXiv:1808.05287].
[13] J. Goodman, A. Dar, S. Nussinov, *ApJ*, 314 (1987) L7.
[14] P. Meszaros, M.J. Rees, *ApJ*, 418 (1993) L59 [arXiv:astro-ph/9309011].
[15] A. von Kienlin, *et al.*, *GCN* 21520 (2017).
[16] V. Savchenko, *et al.*, *ApJL*, 848 (2017) L15 [arXiv:1710.05449].
[17] B.P. Abbott, *et al.*, *PRL*, 119 (2017) 161101 [arXiv:1710.05832].
[18] B.P. Abbott, *et al.*, *ApJ*, 848 (2017) L12 [arXiv:1710.05834].
[19] B.P. Abbott, *et al.*, *ApJ*, 851 (2017) L16 [arXiv:1710.09320].
[20] A. Dar, A. De Rújula, *PHR*, 405 (2004) 203 [arXiv:astro-ph/0308248].
[21] S. Dado, A. Dar, A. De Rújula, *ApJ*, 696 (2009) 994 [arXiv:0809.4776].
[22] S. Dado, A. Dar, (2018) arXiv:1810.03514.
[23] S. Dado, A. Dar, (2017) arXiv:1708.04603.
[24] S. Dado, A. Dar, (2018) arXiv:1807.08726.
[25] S. Dado, A. Dar, (2018) arXiv:1810.03514.
[26] A. Goldstein, *et al.*, *ApJ*, 848 (2017) L14 [arXiv:1710.05446].
[27] K.D. Alexander, *et al.*, (2018) arXiv:1805.02870 and references therein.
[28] K.P. Mooley, *et al.*, (2018) arXiv:1810.12927 and references therein.
[29] A. Dar, A. De Rújula, (2000) arXiv:astro-ph/0012227.
[30] P.N. Bhat, *et al.*, *ApJ*, 744 (2012) 141 [arXiv:1109.4064].
[31] A.S. Pozanenko, *et al.*, *ApJ*, 852 (2018) L30 [arXiv:1710.05448].
[32] S. Dado, A. Dar, (2018) arXiv:1808.08912.
[33] K.P. Mooley, *et al.*, *Nature*, 561 (2018) 355 [arXiv:1806.09693].
[34] M.R. Drout, *et al.*, *Science*, 358 (2017) 1570 [arXiv:1710.054431].
[35] Swift-XRT GRB lightcurve repository. P.A. Evans, *et al.*, *A&A*, 469 (2007) 379 [arXiv:0704.0128], P.A. Evans, *et al.*, *MNRAS*, 397 (2009) 1177 [arXiv:0812.3662].
[36] J. Hjorth, *et al.*, *ApJ*, 848 (2017) L31 [arXiv:1710.05856].
[37] A.G. Riess, *et al.*, *ApJ*, 826 (2016) 56 [arXiv:1604.01424].
[38] I. Mandel, *ApJ*, 853 (2018) L12 [arXiv:1712.03958].